BIOCHEMISTRY
including biophysical chemistry & molecular biology
Article

*Biochemistry* **2010,** *49,* 5269–5277 5269
DOI: 10.1021/bi1006749

# Familial Hypertrophic Cardiomyopathy Can Be Characterized by a Specific Pattern of Orientation Fluctuations of Actin Molecules[†,‡]

J. Borejdo,*[,§] D. Szczesna-Cordary,[∥] P. Muthu,[∥] and N. Calander[⊥]

[§]*Department of Molecular Biology and Immunology and Center for Commercialization of Fluorescence Technologies, University of North Texas Health Science Center, 3500 Camp Bowie Boulevard, Fort Worth, Texas 76107,* [∥]*Department of Molecular and Cellular Pharmacology, University of Miami, Miller School of Medicine, 1600 NW 10th Avenue, Miami, Florida 33136, and* [⊥]*Department of Physics, Macquarie University, Sydney, NSW 2109, Australia*

*Received April 30, 2010; Revised Manuscript Received May 27, 2010*

ABSTRACT: A single-point mutation in the gene encoding the ventricular myosin regulatory light chain (RLC) is sufficient to cause familial hypertrophic cardiomyopathy (FHC). Most likely, the underlying cause of this disease is an inefficient energy utilization by the mutated cardiac muscle. We set out to devise a simple method to characterize two FHC phenotypes caused by the R58Q and D166V mutations in RLC. The method is based on the ability to observe a few molecules of actin in working ex vivo heart myofibril. Actin is labeled with extremely diluted fluorescent dye, and a small volume within the I-band ($\sim 10^{-16}$ L), containing on average three actin molecules, is observed by confocal microscopy. During muscle contraction, myosin cross-bridges deliver cyclic impulses to actin. As a result, actin molecules undergo periodic fluctuations of orientation. We measured these fluctuations by recording the parallel and perpendicular components of fluorescent light emitted by an actin-bound fluorophore. The histograms of fluctuations of fluorescent actin molecules in wild-type (WT) hearts in rigor were represented by perfect Gaussian curves. In contrast, histograms of contracting heart muscle were peaked and asymmetric, suggesting that contraction occurred in at least two steps. Furthermore, the differences between histograms of contracting FHC R58Q and D166V hearts versus corresponding contracting WT hearts were statistically significant. On the basis of our results, we suggest a simple new method of distinguishing between healthy and FHC R58Q and D166V hearts by analyzing the probability distribution of polarized fluorescence intensity fluctuations of sparsely labeled actin molecules.

Familial hypertrophic cardiomyopathy (FHC)[1] is an autosomal dominant disease characterized by ventricular hypertrophy, myofibrillar disarray, and sudden cardiac death (SCD) (*1*). It is believed to be caused by single-point mutations in sarcomeric proteins of the heart. In this report, we have focused on the two FHC mutations in the ventricular regulatory light chain of myosin (RLC) (*2*−*8*), R58Q (arginine 58 replaced by glutamine) and D166V (aspartate 166 replaced by valine). Even though mutations in RLC are less common than mutations in the myosin heavy chain, they are often associated with malignant outcomes. Both RLC mutations, R58Q and D166V, have been shown to cause SCD (*2*−*8*).

Using transgenic (Tg) animal models expressing the R58Q and D166V mutations of RLC, we have determined the effect of these FHC mutations on the ability of the myocardium to develop isometric tension, $Ca^{2+}$ sensitivity of force, and ATPase activity (*9*−*11*). However, such characterization is only possible in a transgenic mouse model, because it usually expresses more than 95% of the mutant protein that replaces the endogenous mouse cardiac RLC. Humans are heterozygous for FHC, so in muscles of affected individuals, 50% of myosin-containing thick filaments are composed of the nonmutant myosin heads interspersed with the FHC mutant heads. If the distribution of the healthy and diseased molecules is random, any collection containing more than a few molecules carries a high probability of containing a mixture of healthy and diseased moieties. It is likely that the gross properties of such muscles will not exhibit any differences compared to those of tissue from healthy individuals. That is why it is important to take measurements from as few molecules as possible. In this paper, we propose a method of characterization of FHC hearts in which histograms of fluctuations of polarized fluorescence of approximately three sarcomeric actin molecules are compared in the mutated versus wild-type (WT) heart muscles.

The method is based on the ability to observe a few molecules of actin in an ex vivo heart muscle, as illustrated in Figure 1 (top). Muscle is labeled with an extremely diluted dye so that only one in ~100000 actin monomers is probed. A small volume within the labeled heart muscle ($\sim 10^{-16}$ L) is observed by confocal microscopy. This volume contains only a few actin molecules (see below). In rigor muscle (left panel), the thin filaments are immobile. There are no fluctuations in orientation of the transition dipole (red arrow). During isometric contraction (right panel), the situation is quite different. Now, myosin cross-bridges deliver impulses to actin (*12*). The force impulses deform the actin filament,

[†]Supported by National Institutes of Health Grants R01AR048622 (to J.B.), R01HL071778 (to D.S.-C.), and R01HL090786 (to J.B. and D.S.-C.).

*To whom correspondence should be addressed. Telephone: (817) 735-2106. Fax: (817) 735-2118. E-mail: Julian.Borejdo@unthsc.edu.

[1]Abbreviations: FHC, familial hypertrophic cardiomyopathy; RLC, regulatory light chain of myosin; R58Q, mutation in which arginine 58 is replaced by glutamine; D166V, mutation in which aspartate 166 is replaced by valine; LV, left ventricle; Tg, transgenic; DV, detection volume; RP, rhodamine-phalloidin; HS, half-sarcomere; APD, Avalanche photodiode.


Published on Web 05/28/2010

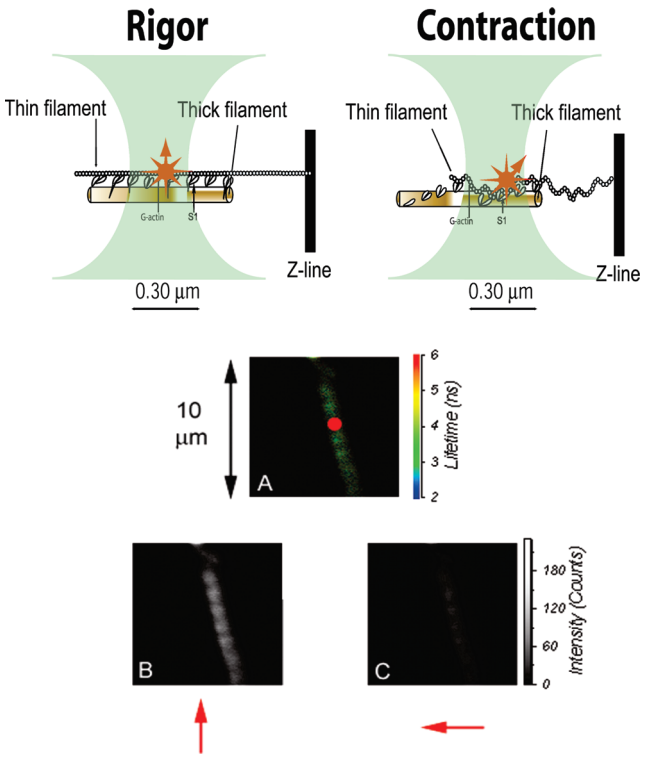


FIGURE 1: Origin of fluctuations (top). Actin is labeled with extremely diluted fluorescent dye (red star) and is placed in the center of the confocal volume of a confocal microscope. The waist of this detection volume (DV) is 1.2 $\mu$m and is equal to the diameter of the confocal pinhole ($2\omega_o$ = 50 $\mu$m) divided by the magnification of the objective (40×). The DV is assumed to be an ellipsoid of revolution with a waist $\omega_o$ and height $z_o$ equal to the thickness of a typical myofibril. If we take this thickness to be 1 $\mu$m, DV = $^4/_3\pi\omega_o^2 z_o \sim 1\ \mu m^3$. This is approximately equal to the volume of a half-sarcomere with typical values for length, width, and height of 1, 1, and 1 $\mu$m, respectively. Therefore, the signal detected by the instrument is contributed by the fluorescent molecules in one half-sarcomere. In rigor muscle (left panel), the thin filaments are stationary. There are no fluctuations in orientation of the transition dipole (red arrow). During isometric contraction (right panel), myosin cross-bridges deliver impulses to actin which deform the actin filament, changing the orientation of a transition dipole of rhodamine. The orientation of the rhodamine dipole fluctuates in time. In addition, fluctuations arise because rhodamine may leave and re-enter the observational volume, as cross-bridges pull filaments to the left, and filaments recoil during isometric contraction to the right. We measure fluctuations by recording parallel (∥) and perpendicular (⊥) components of fluorescent light emitted by an actin-bound fluorophore. The bottom panels show lifetime (A) and polarization (B and C) images of the rigor Tg-WT myofibril from the mouse right ventricular muscle. The color bar at the right of panel A is the lifetime scale, with red corresponding to 6 ns and blue to 2 ns. The red circle is the projection of the confocal aperture on the sample plane. Its diameter (1.2 $\mu$m) is equal to the diameter of the confocal aperture (50 $\mu$m) divided by the magnification of the objective (40×). The black and white intensity scale is 0−255, with 255 corresponding to white and 0 to black. Red arrows indicate the direction of polarization of the fluorescent light. The exciting light is polarized vertically. Myofibrils were labeled with 1 $\mu$M Alexa488-phalloidin. The sarcomere length was 2.2 $\mu$m. Images were acquired with the PicoQuant Micro Time 200 confocal lifetime microscope. Excitation with a 470 nm pulse of light, emission through an LP500 filter.

changing the orientation of a transition dipole of rhodamine. The orientation of this rhodamine dipole fluctuates in time. In addition, fluctuations arise because rhodamine may leave and re-enter the observational volume, as cross-bridges pull filaments to the left, and filaments recoil during isometric contraction to the right. We measure fluctuations by recording parallel (∥) and perpendicular (⊥) components of fluorescent light emitted by an actin-bound fluorophore. The ratio of these components, called polarized fluorescence, is a sensitive indicator of the orientation of the transition dipole of the fluorophore (*13*−*20*). It is worth pointing out that the current method does not rely on computing the correlation function of fluctuations. Although sophisticated and elegant (*21*, *22*), the correlation analysis is complex and depends on a number of assumptions, which are avoided here. The current method involves only the elementary statistical analysis.

It is advantageous to observe actin rather than myosin because labeling of actin with fluorescent phalloidin was shown not to alter the enzymatic properties of skeletal muscle (*23*, *24*), labeling is stoichiometric and thus allows for a strict control of the degree of labeling, and actin is labeled noncovalently and therefore rigidly. Rigid binding is a must when the orientation of the dipole moment of a probe is measured.

The fluctuations of WT rigor heart muscles were distributed according to a perfect Gaussian curve in which both the skewness and kurtosis of the distribution approach zero. In contrast, the histograms of contracting heart muscles were peaked and asymmetric (i.e., they had high skewness and kurtosis), suggesting that contraction occurred in at least two steps. Moreover, the differences between histograms of contracting FHC mutated and WT heart muscles were statistically significant. These results suggest that a simple way to distinguish between FHC hearts carrying R58Q and/or D166V mutations from WT hearts is to analyze the probability distribution of polarized intensity fluctuations.

## MATERIALS AND METHODS

*Chemicals and Solutions*. Rhodamine-phalloidin (RP) and Alexa488-phalloidin were purchased from Molecular Probes (Eugene, OR). All other chemicals were from Sigma-Aldrich (St. Louis, MO). The compositions of solutions were as described in ref *25*.

*Transgenic Muscle*. The hearts from Tg-WT and Tg-R58Q male mice of various ages were used for the preparation of glycerinated muscle strips. Skinned fiber measurements were performed as described previously (*25*). Myofibrils, prepared as described in ref *25*, were labeled with 0.1 nM rhodamine-phalloidin (RP) and 10 $\mu$M unlabeled phalloidin (UP) in $Ca^{2+}$-rigor solution as described in ref *26*. Because the ratio of fluorescent to nonfluorescent phalloidin was 1:100000, only one in $\sim 10^5$ actin monomers carried a fluorophore. Myofibrils were prevented from shortening during contraction by cross-linking with the water-soluble cross-linker EDC (*27*). Myofibrils (1 mg/mL) were incubated with 20 mM EDC for 20 min at room temperature. The reaction was stopped via addition of 20 mM DTT. The lack of shortening was checked under differential contrast (*28*).

*Coverslips*. Cardiac myofibrils attached weakly to glass. To help them attach, the coverslips were thoroughly cleaned with 100% ethanol and spin coated with a poly-L-lysine solution (0.1%, Sigma-Aldrich) at 3000 rpm for 120 s using a P6700 spincoater (Specialty Coating Systems, Indianapolis, IN).

*Probability Distribution Measurements*. An Alba-FCS (ISS Co., Urbana, IL) confocal system coupled to an Olympus IX 71 microscope was used to obtain fluorescence data. Fluorescence was collected every 10 $\mu$s for 20 s (2 M data points). The signal was smoothed by binning 1000 data points (final frequency

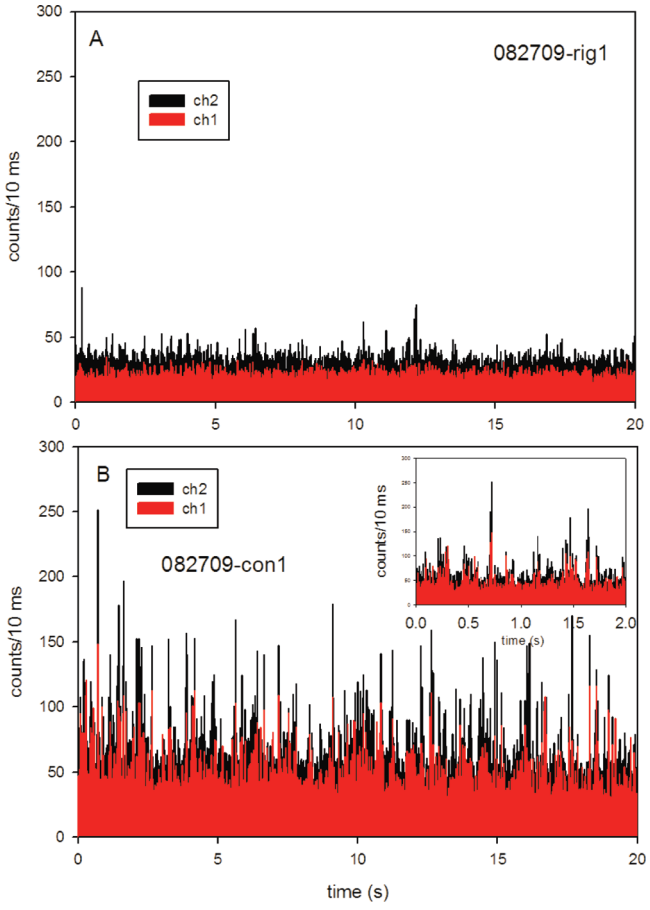


FIGURE 2: Time course of polarized intensity of a rigor WT (A) or contracting (B) myofibril from the left ventricle of a Tg-WT heart. The original data were collected every 10 $\mu$s, and 1000 points are binned together to give a time resolution of 10 ms. This is a bar plot, where the vertical scale is the number of counts during 10 ms. Ch1 (red) and Ch2 (black) are the fluorescence intensities polarized perpendicular ($I_\perp$) and parallel ($I_\parallel$) to the myofibrillar axis, respectively. The myofibrillar axis is vertical on the microscope stage. The inset of panel B shows the time course on a 0−2 s time scale.

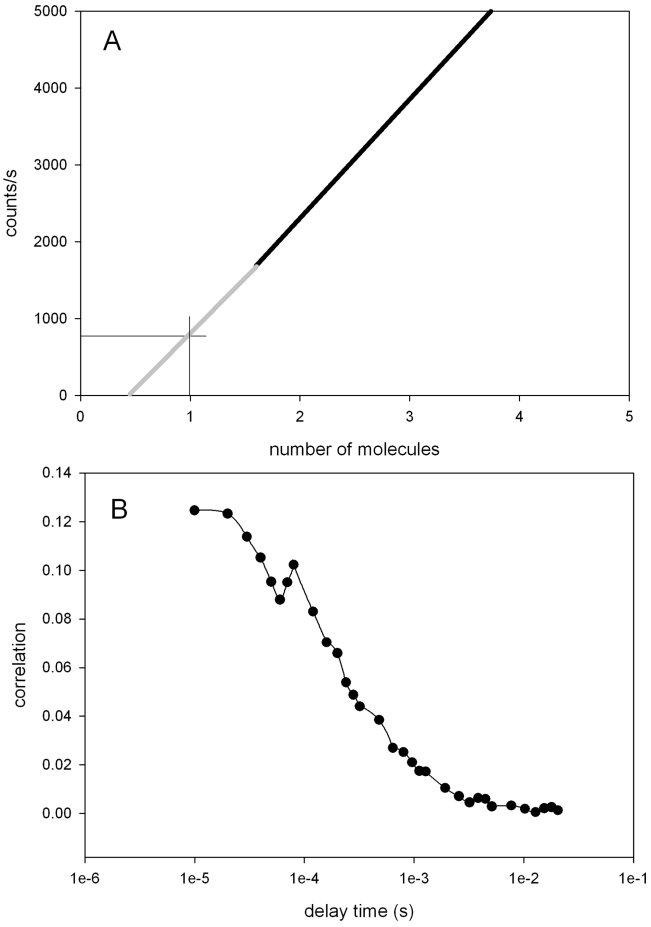


FIGURE 3: Estimation of the number of observed molecules. (A) Measured intensity of the signal at increasing concentrations of rhodamine B in solution. The signal intensity of a 0.5−50 nM solution of rhodamine B was plotted vs the number of molecules in the DV. For example, when the dye concentration was 5 nM, the signal measured in channel 1 and 2 was averaged to 99 and 115 counts per 10 ms. The curve was extrapolated as shown by the gray line, from which the number of photons per one fluorophore was estimated to be ~800 counts/s per channel. The number of molecules contributing to the signal was measured by recording the autocorrelation function associated with each signal. The value of the autocorrelation function at delay time 0 [$G(0)$] is equal to an inverse of the number of molecules $N$ contributing to the signal [$N = 1/G(0)$]. The autocorrelation function of the signal of 5 nM rhodamine B is shown in panel B. $G(0)$ was 0.127, giving approximately eight molecules.

response of 100 Hz). Before each experiment, the instrument was calibrated and optimized with a 50 nM solution of rhodamine G. Excitation was achieved with a 532 nm CW laser. The linearly polarized laser beam was delivered by single-mode fiber, but to ensure that the exciting light was polarized, a sheet analyzer was inserted before the entrance to the microscope. The laser polarization was vertical on the microscope stage. The confocal pinhole was 50 $\mu$m. The fluorescent light was split by a prism, and each component was detected by a separate Avalanche photodiode (APD). Orthogonally polarized linear analyzers were placed before APD's. The myofibrils were always placed with the axis pointing vertically on the microscope stage. Channels 1 and 2 measured the polarized intensities oriented perpendicular and parallel to the myofibrillar axis, respectively.

*Anisotropy Decay*. To ascertain whether the phalloidin probe is immobilized by the protein so that the transition dipole of the fluorophore reflects the orientation of the protein, we measured the decay of anisotropy, defined by the relationship $r = (I_\parallel - I_\perp)/(I_\parallel + 2I_\perp)$. It was best fitted by the exponential function $r(t) = R_\infty + a \times \exp(-t/\theta)$, where $R_\infty$ (0.29) is the value of anisotropy at infinite time, $a$ (0.07) is the amplitude of the anisotropy change, and $\theta$ (1.3 ns) is the rotational correlation time. The short correlation time was due to the rotation of phalloidin, consistent with rotation of an $M_w = 1250$ molecule. The maximum value of anisotropy was 0.35. It decayed to an asymptotic value of $R_\infty$ (0.29). Thus, the mobile fraction was contributed by (35% − 29%)/35% = 17% of fluorophores; 100% − 17% = 83% of fluorescent phalloidin was immobilized by F-actin. This is consistent with the fact that phalloidin attaches to F-actin through long-range interactions that impart on a probe the rigidity necessary for quantitative polarization measurements.

*Steady-State Force Measurements*. Skinned papillary muscle fibers from Tg-R58Q and Tg-D166V mice were used to assess the effect of the mutation on maximal force compared to that of Tg-WT. A bundle of fibers with an approximate diameter of 100 $\mu$m was isolated from a batch of glycerinated mouse papillary muscle fibers and attached by tweezer clips to a force transducer (*29*). The fibers were relaxed in 1 mL of a pCa 8 solution and then tested for maximal steady-state force in pCa.

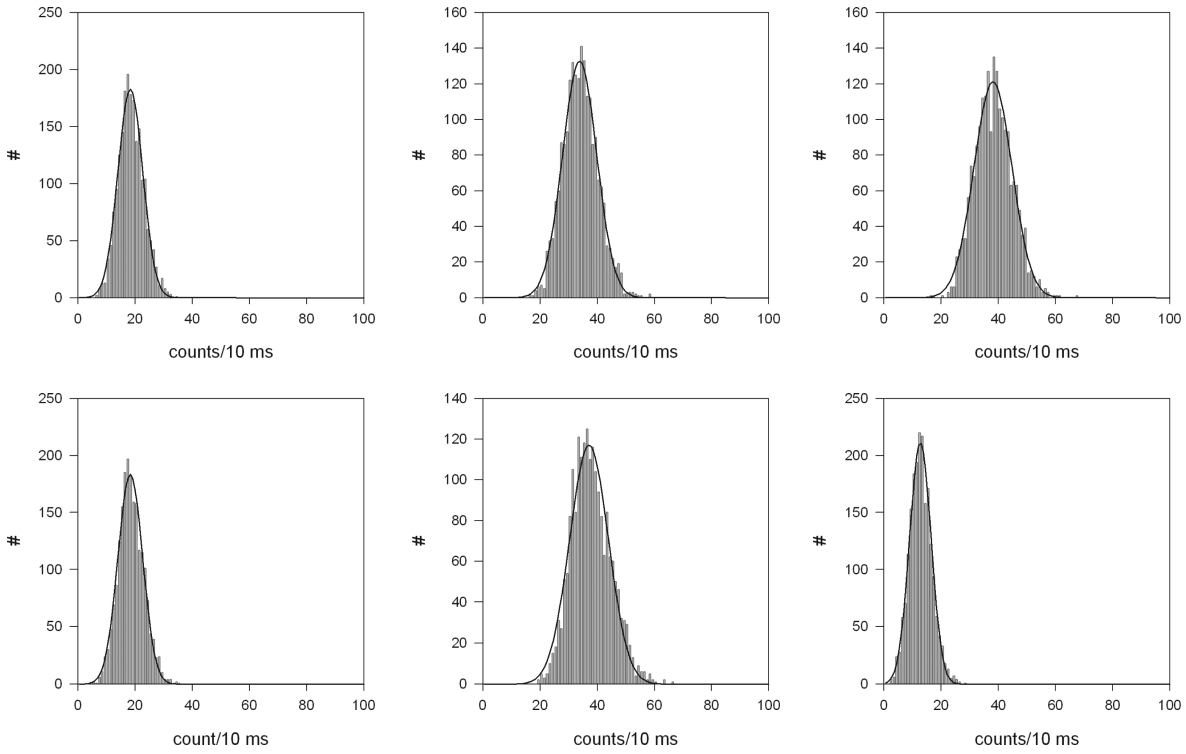


FIGURE 4: Examples of histograms of $I_{\perp}$ of rigor WT myofibrils. The solid line shows the fit to the three-parameter Gaussian $y = a\exp[-0.5(x - x_o/b)^2]$. Left ventricle muscle.

## RESULTS

*Imaging*. A typical fluorescence lifetime image of a rigor Tg-WT myofibril from the right ventricle of mouse heart is shown in Figure 1 (bottom). Panel A shows the lifetime image (the lifetime image is shown because it is of better quality than the intensity image). The entire I-bands are labeled because heart muscle does not contain nebulin. In skeletal muscle, nebulin prevents phalloidin from labeling all but the pointed ends of actin filaments (*30*, *31*). As expected, the intensity of fluorescence in Z-lines is approximately double that in the I-band (*32*). The dark areas are the H-bands that do not contain actin. The red circle is a two-dimensional projection of the confocal aperture on the image plane. Its diameter is equal to the diameter of the confocal aperture (50 $\mu$m) divided by the magnification of the objective (40×). The parallel ($I_{\parallel}$) and perpendicular ($I_{\perp}$) polarization images are shown in panels B and C of Figure 1, respectively. They show that fluorescence is highly anisotropic, which is expected from the aligned array of polar actin filaments (*32*).

*Intensity Fluctuations during Rigor and Contraction of Healthy Hearts*. We first measured the time course of polarized intensities of rhodamine-phalloidin (RP) bound to an actin filament in a cardiac half-sarcomere (HS). Since rhodamine is rigidly immobilized on the surface of actin (*25*), the polarized intensity reflects the orientation of actin. A myofibril is placed on the stage of a confocal microscope. Its axis is always vertical on a microscope stage. The linear polarization of the illuminating laser light is also vertical on a stage (i.e., it is parallel to muscle axis). The fluorescence emanating from the detection volume (DV) is split 50:50 by a beam splitter and projected through the confocal apertures and orthogonal analyzers on the photosensitive surface of two APD's. The signals in the first (channel 1) and second (channel 2) channel of the APD correspond to the intensities of fluorescence polarized perpendicular ($\perp$) and parallel ($\parallel$) to the muscle axis, respectively. Figure 2 shows a typical time course of perpendicularly polarized intensity of a rigor (A) and contracting (B) myofibril from the left ventricle of a Tg-WT heart. The original data were collected every 10 $\mu$s, but to keep the data files to a manageable size, 1000 points were binned together to give a time resolution of 10 ms. The vertical scale is the number of counts during 10 ms. Individual impulses resulting from the myosin cross-bridge imparting force impulses on actin can be clearly seen. The impulses can be even better visualized on the expanded time scale (inset).

*Number of Observed Molecules*. For the meaningful interpretation of histograms, it is important that the data originate from only a few molecules. If it were not, asynchrony between cross-bridges would have averaged out the fluctuations, and no asymmetry would have been visible. To be able to assess how many molecules contribute to the observed fluorescence, it is necessary to know the photon rate associated with a single molecule. To this end, we measured the intensity of a signal at increasing concentrations of rhodamine B in solution. To estimate the number of molecules contributing to the signal, we measured the associated autocorrelation function. The value of the autocorrelation function at delay time 0 [$G(0)$] is equal to the inverse of the number of molecules $N$ contributing to the signal [$N = 1/G(0)$ (*33*, *34*)]. Correlation functions were obtained for the solution of rhodamine B in the range of 0.5−50 nM. For example, when the dye concentration was 5 nM, the signal measured in channels 1 and 2 averaged to 99 and 115 counts per 10 ms. The autocorrelation function of the signal is shown in Figure 3B. $G(0)$ was 0.127, giving approximately eight molecules. The amplitude of the signal was plotted versus the average number of molecules in the DV (Figure 3A). The straight line curve was extrapolated as shown by the red line in Figure 3A, and from this, the number of photons per fluorophore was estimated to be ~800 counts/s per channel.

We can now estimate the number of molecules contributing to the signal. In Figure 2, the average intensities in contracting myofibrils in channels 1 and 2 were 19 and 29 counts per 10 ms for rigor and 43 and 60 counts per 10 ms, respectively (note that Figure 2 is a bar plot). The number of excess counts for contracting muscle, which takes into account the contribution of the background, was on average 27 counts/10 ms = 2700 counts/s. This corresponds to approximately three actin molecules.

*Histograms of Fluctuations*. A histogram is a plot of the size of fluctuation ($x$-axis) versus the number of times that a given fluctuation occurs ($y$-axis). We compared the histogram distributions of rigor and contracting myofibrils. Figure 4 shows examples of six histograms obtained from the left ventricles of rigor WT hearts, randomly selected from a pool of 262 histograms. It is clear that the three-parameter Gaussian relationship $y = a \exp[-0.5(x - x_o/b)^2]$ fits the data well. As mentioned previously, the Gaussian distribution is characterized by a skewness and kurtosis of zero. Rigor histograms (from left to right and top and bottom) had skewness values of 0.234, 0.249, 0.208, 0.252, 0.369, and 0.278 with an average of 0.265 ± 0.055 (standard deviation). Kurtosis values were 0.018, 0.170, 0.048, 0.153, 0.144, and 0.247 with an average of 0.130 ± 0.084 (standard deviation). These values are reported in Table 1. The fact that both kurtosis and skewness were close to 0 suggests that fluctuations in rigor muscle reflected a stationary process whose magnitude was controlled solely by random fluctuations in an APD current.

Table 1: Comparison of Kurtosis and Skewness of Rigor and Contracting Tg-WT Left Ventricular Muscle[a]

| | kurtosis | skewness | $N$ |
|---|---|---|---|
| rigor | 0.130 ± 0.084 | 0.265 ± 0.055 | 262 |
| contraction | 4.562 ± 1.605 | 1.571 ± 0.286 | 262 |

[a]Errors are standard deviations, and $N$ is the number of experiments.

In contrast, corresponding histograms of $I_\perp$ fluctuations obtained from contracting left ventricles from Tg-WT hearts were heavily right-shifted (Figure 5). The histograms had high positive skewness values of 1.701, 1.767, 1.916, 1.372, 1.129, and 1.543 (left to right and top and bottom), with an average of 1.571 ± 0.286 (standard deviation). Kurtosis values were 4.240, 5.897, 5.946, 2.859, 2.492, and 5.939, with an average of 4.562 ± 1.605 (standard deviation) reflecting a substantial number of large fluctuations. The differences between the rigor and contraction data were statistically highly significant ($p < 0.001$, $t = 9.503$, paired $t$ test for skewness; $p = 0.001$, $t = 6.790$, paired $t$ test for kurtosis). The results are summarized in Table 1.

The marked skewness and kurtosis of polarized intensity during contraction are probably due to the fact that a cross-bridge power stroke affects the orientation of actin in two or more steps, as originally proposed by Huxley and Simmons (*35*). Our results suggest that unwinding of the 'kink' in the relay helix of the converter domain of myosin head (*36*), may occur in discrete steps.

The asymmetric contracting data could be fitted by a mixture of two Gaussian curves, with the dominant curve containing most of the power, centered significantly to the left of the secondary Gaussian. Figure 6 represents a pair of Gaussian curves with the experimental curve, labeled in blue (data from Figure 5, top left) fitted with the dominant Gausssian curve (mean ± standard deviation, 37.1 ± 7.9; 74% contribution, red)

$$f_1(x) = \frac{1}{\sqrt{2\pi}}\left\{\frac{0.7377}{7.906}\exp\left[-\frac{(x-37.092)^2}{2\times 7.906^2}\right]\right\}$$

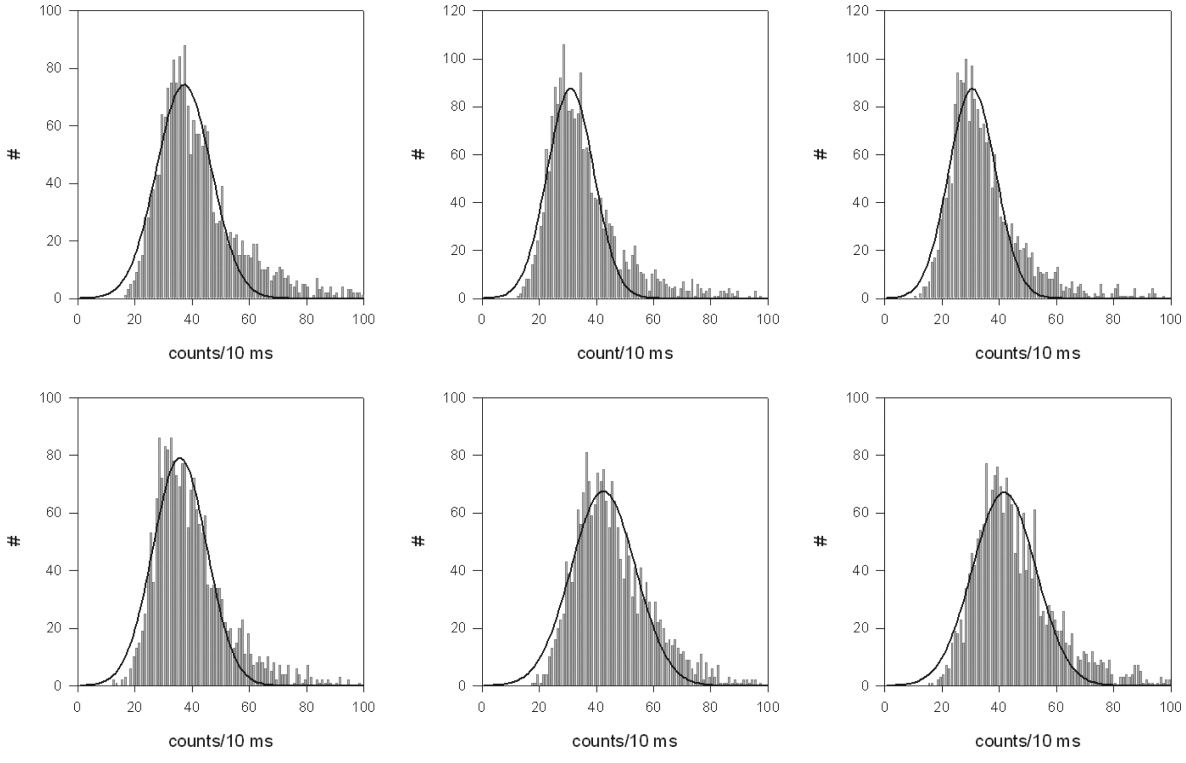


FIGURE 5: Examples of histograms of $I_\perp$ of contracting WT myofibrils. The solid line shows the fit to the three-parameter Gaussian $y = a \exp[-0.5(x - x_o/b)^2]$. LV muscle.

and the secondary Gaussian curve (labeled in green) fitted with (mean ± standard deviation, 60.5 ± 19.2; 26% contribution)

$$f_2(x) = \frac{1}{\sqrt{2\pi}}\left\{\frac{0.2623}{19.161}\exp\left[-\frac{(x-60.510)^2}{2\times 19.161^2}\right]\right\}$$

The overall fitted curve is given by the sum of these two equations. The relative contribution of both Gaussian curves was 74% (dotted line) and 26% (dashed line).

*Intensity Fluctuations of Contracting Myofibrils from Tg-R58Q and Tg-D166V Mutated Hearts*. From the previous section, it appears that the analysis of histograms can distinguish between the resting and active myofibrils from Tg-WT hearts. The question arises of whether the same analysis of contracting heart muscles is capable of predicting whether the heart muscle carries an FHC-causing mutation. Figure 7 shows six randomly picked histograms obtained from fluctuations of R58Q mutated Tg myofibrils. The histograms are also right-shifted. A careful comparison of 98 perpendicular and 120 parallel histograms of fluctuations in the intensity of fluorescence originating from contracting Tg-WT and Tg-R58Q myofibrils reveals a statistically significant difference. The comparisons were performed on myofibrils from left and right ventricles or papillary muscles from age-matched Tg-WT and Tg-R58Q male mice. The absolute values were (mean ± standard error) 5.2 ± 0.5 and 3.9 ± 0.4 for kurtosis and 1.5 ± 0.07 and 1.2 ± 0.06 for skewness for Tg-WT and Tg-R58Q mutated hearts, respectively. The differences in kurtosis and skewness were statistically significant at a $<10\%$ level for kurtosis ($t = 1.860$, $p = 0.064$) and at a $<5\%$ level for skewness ($t = 2.955$, $p = 0.003$). The results are summarized in Figure 8 and Table 2. We also analyzed 20 and 16 histograms of fluctuations in perpendicular and parallel polarized intensity, respectively, from myofibrils of left ventricles carrying the D166V FHC mutation. The absolute values were 1.2 ± 0.4 and 2.2 ± 0.4 for kurtosis and 0.6 ± 0.09 and 1.0 ± 0.1 for skewness for Tg-WT and Tg-D166V mutated hearts, respectively. The differences were statistically significant at an ~10% level for kurtosis ($t = -1.639$, $p = 0.110$) and at a $<5\%$ level for skewness ($t = -3.267$, $p = 0.002$). In this case, in contrast to R58Q result, the values of kurtosis and skewness were greater for the mutated myofibrils compared to WT muscle. The results are summarized in Figure 9 and Table 2.

*Functional Studies. Maximal Level of Steady-State Force*. Figure 10 demonstrates the effect of both mutations, D166V and R58Q, on the maximal force per cross-sectional area of muscle developed in mouse skinned papillary muscle fibers

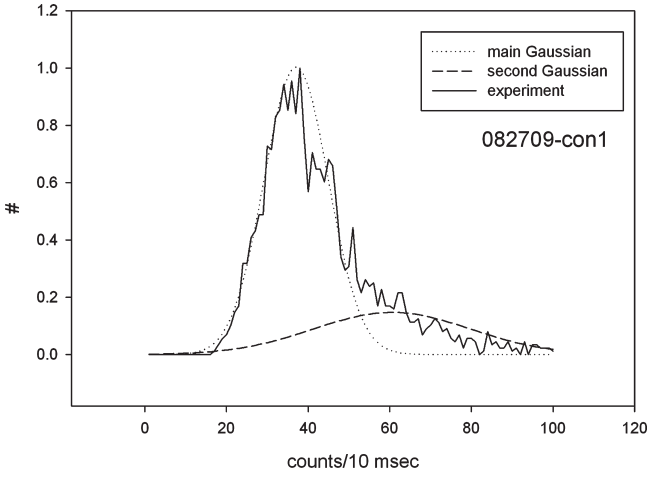


FIGURE 6: Fit of the experimental curve (—) (data from Figure 5, top left) with the main Gaussian curve (· · ·) (mean ± standard deviation, 37.1 ± 7.9, red) and a secondary one (---) (mean ± standard deviation, 60.5 ± 19.2, green). The relative contributions are 74% (main) and 26% (secondary).

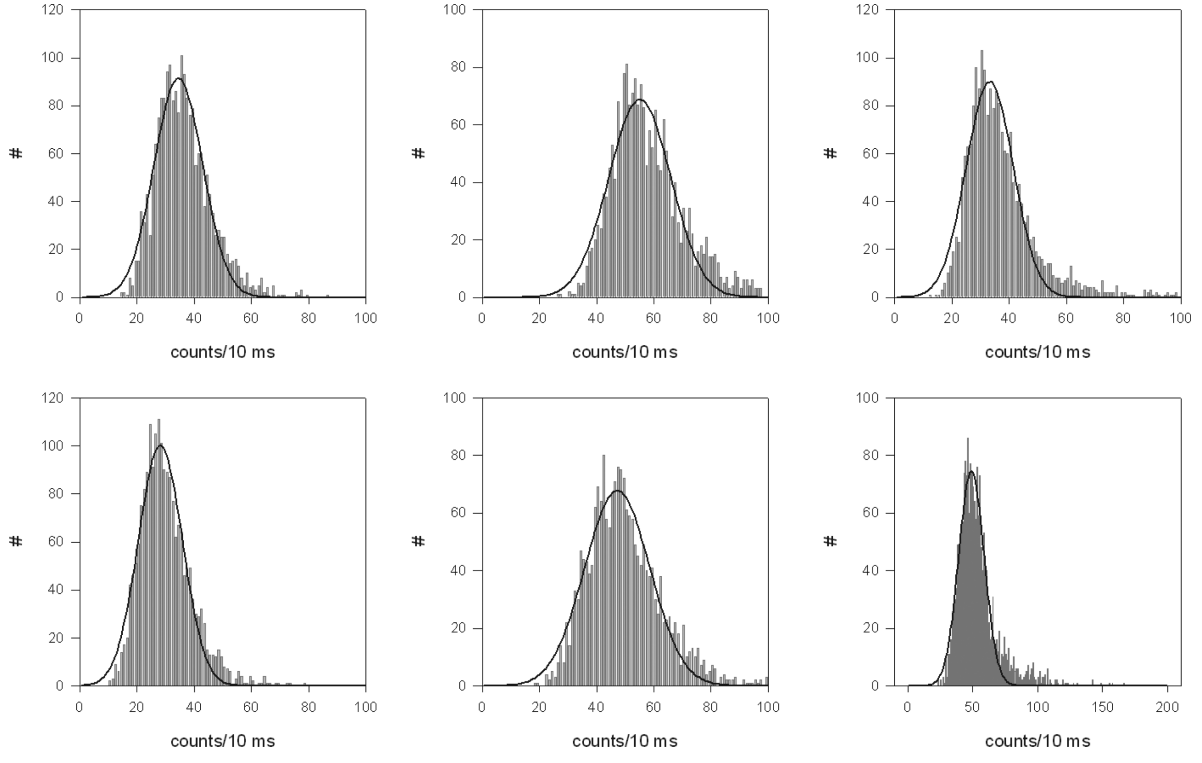


FIGURE 7: Examples of histograms of $I_\perp$ of contracting R58Q myofibrils. The solid line shows the fit to the three-parameter Gaussian $y = a \exp[-0.5(x - x_o/b)^2]$. LV muscle.

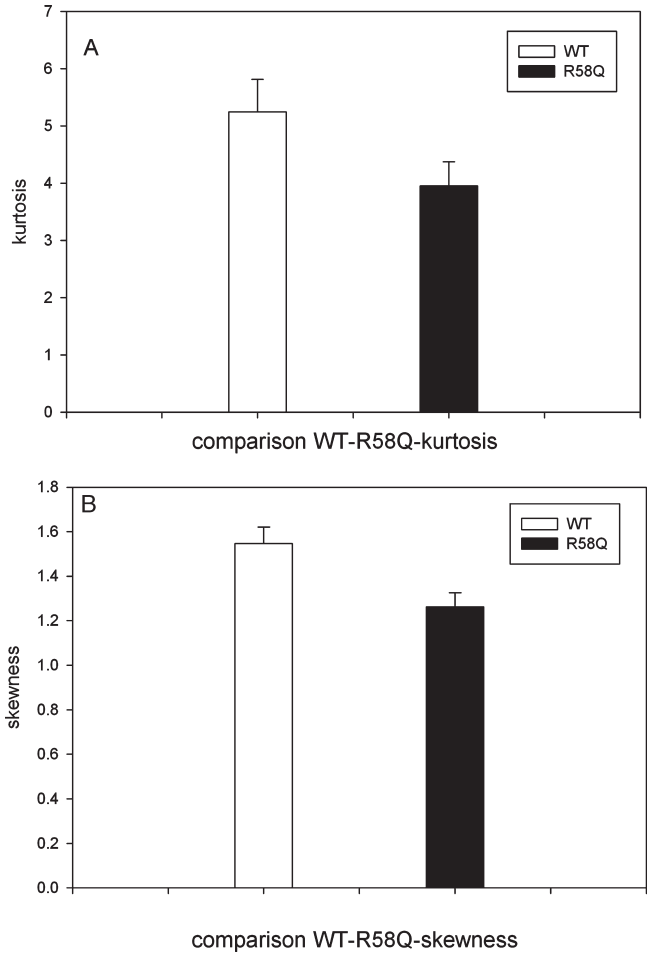


FIGURE 8: Comparison of average values of kurtosis (A) and skewness (B) for R58Q hearts.

Table 2: Comparison of Kurtosis and Skewness of Contracting Tg-WT and Tg-Mutant Myofibrils[a]

| transgenic muscle | kurtosis | skewness | *N* |
|---|---|---|---|
| WT (R58Q) | 5.2 ± 0.5 | 1.5 ± 0.07 | 218 |
| R58Q | 3.9 ± 0.4 | 1.2 ± 0.06 | 218 |
| WT (D166V) | 1.2 ± 0.4 | 2.2 ± 0.4 | 36 |
| D166 V | 0.6 ± 0.09 | 1.0 ± 0.1 | 36 |

[a]Errors are standard errors, and *N* is the number of experiments.

from female mutant mice compared to control, age-matched Tg-WT mice. The value of maximal force determined at high $Ca^{2+}$ concentrations (pCa 4) in Tg-D166V fibers was decreased by 28% compared to that of Tg-WT fibers ($p = 0.037$). Interestingly, Tg-R58Q fibers demonstrated a 3.3-fold decrease in force compared to that of Tg-WT fibers ($p = 0.001$) and a 2.3-fold decrease compared to that of Tg-D166V fibers ($p < 0.001$). Therefore, both mutations, D166V and R58Q, led to the compromised development of force in these mutated hearts, ultimately resulting in compensatory hypertrophy.

## DISCUSSION

*Skewness and Kurtosis during Rigor and Contraction*. A histogram can be quantitatively characterized by the values of kurtosis and skewness. A positive skewness means that the tail of the curve is directed toward positive values of the histogram,

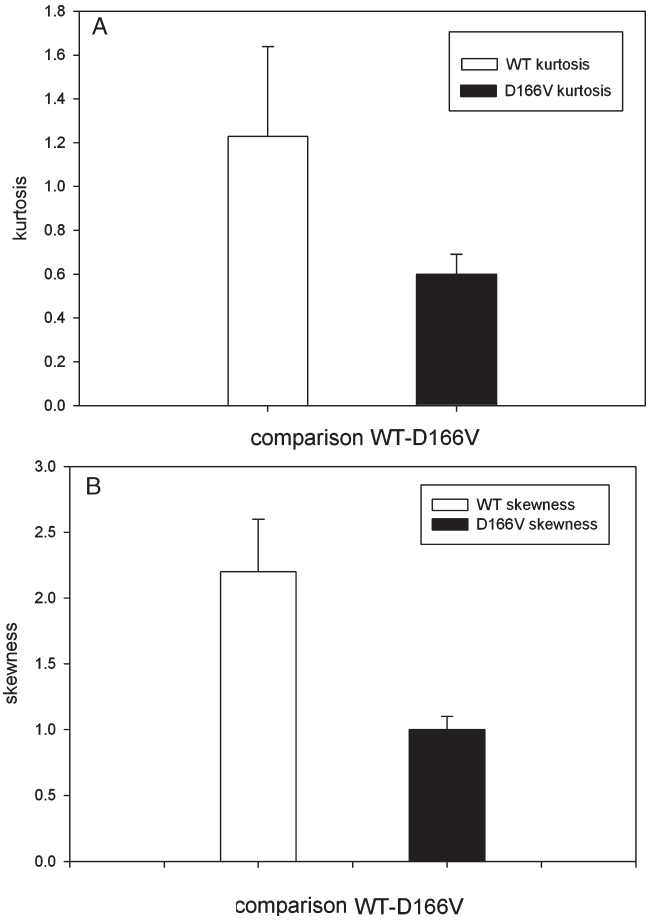


FIGURE 9: Comparison of average values of kurtosis (A) and skewness (B) for D166V hearts.

while in the negative skewness, the tail goes toward the negative values. A positive kurtosis is expressed by long tails compared to the Gaussian curves, and a negative kurtosis means that the tails are smaller than those of Gaussian curves. The skewness and kurtosis are defined by eqs 1 and 2.

$$\text{skewness} = \frac{\mu_3}{\sigma^3} \quad (1)$$

$$\text{kurtosis} = \frac{\mu_4}{\sigma^4} - 3 \quad (2)$$

where $\sigma = [(1/N)\sum_{n=1}^{N}(x_n - \bar{x})^2]^{1/2}$ is the standard deviation of the $N$ values $x_n$ with the mean $\bar{x}$ and the moments $\mu_m$ are defined by $\mu_m = (1/N)\sum_{n=1}^{N}(x_n - \bar{x})^m$. This is illustrated in Figure 11.

*Skewness and Kurtosis of FHC Heart Myofibrils*. We observed significant differences in the histogram shape of rigor and contracting myofibrils from transgenic mouse hearts containing WT RLC (Figures 5 and 6 and Table 1). The difference in histograms was not limited to rigor and contracting muscles. We observed a statistically significant difference between skewness and kurtosis of fluctuations during contraction of Tg-WT (healthy) and Tg-mutant (diseased) hearts (Figures 9 and 10 and Table 2). While the difference was not as obvious as that between the rigor and contracting myofibrils, it was statistically significant.

*Implications for Heart Studies*. In our transgenic mouse myocardium, the mutated human ventricular RLC WT replaces the endogenous mouse ventricular RLC in ~95% of the cases. Likewise, Tg-D166V and Tg-R58Q mice express ~95% transgene, and the transgenic mutant myocardium contains ~95%

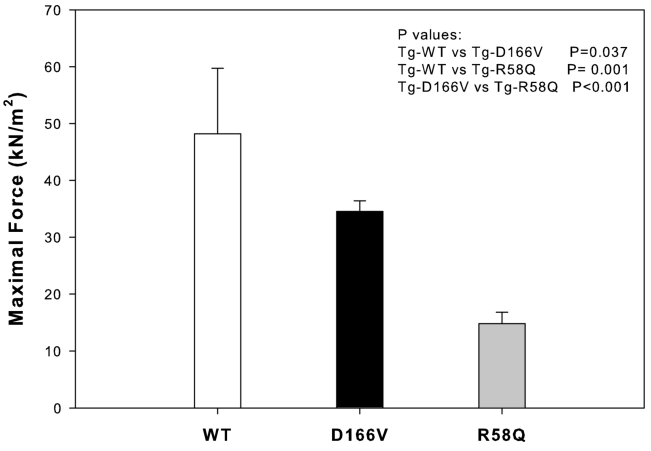


FIGURE 10: Maximal steady-state force measured in skinned papillary muscle fibers from Tg-D166V and Tg-R58Q mice compared to Tg-WT mice. The values of force (in kilonewtons) per cross-sectional area (in square meters) of fibers were 48.17 ± 11.55 (standard deviation) ($n$ = 9 fibers) for Tg-WT, 34.51 ± 1.88 (standard deviation) ($n$ = 4 fibers) for Tg-D166V, and 14.79 ± 1.97 (standard deviation) ($n$ = 7 fibers) for Tg-R58Q.

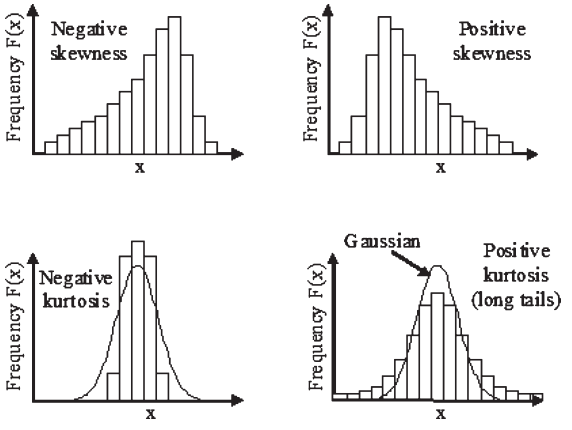


FIGURE 11: Definition of skewness and kurtosis.

mutated RLC incorporated into their myofilaments. In such hearts, it is possible to detect differences between Tg and WT muscles by the simple measurement of tension as presented in Figure 11. In agreement with our previous studies (*9*, *11*), maximal steady-state force development was significantly impaired in Tg mutant hearts, with the R58Q mutation causing the most dramatic effect (Figure 10). Similarly, it was possible to show differences between the WT and mutated hearts using the surface plasmon effect in a population containing many labeled molecules (*37*). However, human patients harboring these FHC RLC mutations are usually heterozygous, and their myosin-containing thick filaments contain ~50% of the mutant myosin heads interspersed with ~50% of the nonmutated myosin cross-bridges. Because of this heterozygous assembly of molecules, the information about the differences in the functional characterization of their muscles might be lost unless the diseased muscle manifests a poison-peptide effect (*38*). The necessity of studying the FHC-linked disease by observing a single molecule or, at most, a few molecules becomes apparent. Even if our data originate from more than one molecule, they all reside in the same HS and are likely subjected to an FHC mutation.

Compared with those of WT hearts, skewness and kurtosis were decreased in both R58Q and D166V hearts. We want to emphasize that no correlation analysis of the kinetic data was used here. This is a significant advantage of this method, because the correlation analysis requires that a specific model of cross-bridge−actin interaction be assumed. For example, the decay of the autocorrelation function can be fitted with a single parameter $\kappa$. Using a single-exponential fit of the autocorrelation function, we found an increase in $\kappa$ from 69 $s^{-1}$ for WT hearts to 169 $s^{-1}$ for R58Q mutated hearts. The same analysis applied to the D166V mutation revealed that the median rate increased from 58 $s^{-1}$ for WT hearts to 102 $s^{-1}$ for D166V mutated hearts. The similar behavior of these two mutations is consistent with the fact that both mutations demonstrated a similar effect on the maximal steady-state force measured in skinned papillary muscle fibers (Figure 10). The results obtained with the R58Q mutation are consistent with studies by Greenberg et al. in which myosin purified from R58Q hearts showed higher actin-activated ATPase rates (0.63 $s^{-1}$) than the controls (0.43 $s^{-1}$) (*39*). In addition, Tg-R58Q myosin showed an increase in actin filament sliding velocity in an in vitro motility assay (2.17 $\mu$m/s) compared to Tg-WT (1.57 $\mu$m/s) (*39*). Our recent surface plasmon microscopy study using Reverse Kretschmann excitation confirmed that faster cross-bridge kinetics are associated with the R58Q mutation (*37*).

The single-exponential fit of the correlation function for the D166V mutant myofibrils results in a larger value of kinetic constant $\kappa$ compared to the fit for WT (58 $s^{-1}$ for WT hearts increased to 102 $s^{-1}$ for D166V mutated hearts). These findings appear to be in conflict with the results of our earlier work (*25*), in which the autocorrelation function was fitted with a train of triangles model, giving the times when the cross-bridges were accessible ($t_A$) or unaccessible ($t_U$) for binding to actin. In work by Muthu et al., we found that $t_A$ was profoundly increased in D166V versus WT and that the cycle times, $t_{on}$ and $t_{off}$, were increased or not changed in D166V muscle compared to WT. This suggests that the value of kinetic constant $\kappa$ as well as the times $t_A$, $t_U$, $t_{on}$, and $t_{off}$ are all model-specific.

Interestingly, the similar effect of both mutations was found in functional studies as they both decreased the maximal steady-state force in skinned papillary muscle fibers (Figure 10). In conclusion, the increase in the $\kappa$ value, the decrease in force development (Figure 10), the small increase in ATPase activity (data not shown), and the retardation of relaxation all argue for the fact that mutations may have caused changes in cross-bridge kinetics by shifting the rate-limiting step of the cross-bridge cycle from the release of ADP/$P_i$ to the release of cross-bridges from actin.

We suggest that when placed in vivo both mutations would lead to compensatory hypertrophy and inefficient workings of the heart. It seems that a larger change in myosin cross-bridge kinetics leads to a more severe force phenotype since the difference in maximal force between WT and R58Q muscle fibers was much larger than that between WT and D166V mutant fibers (Figure 10). Both mutations were reported to cause malignancy in humans, but the R58Q mutation was associated with multiple cases of sudden cardiac death in a few ethnically different families (*3*, *5*−*7*). The strength of the few-molecule method presented here includes the ability to clearly determine the kinetic properties of the myosin cross-bridges from healthy and FHC individuals.

## ACKNOWLEDGMENT

We thank Dr. S. Chen (University of North Texas Health Science Center, School of Public Health) for help with data analysis.

## REFERENCES


1. Maron, B. J. (2002) The young competitive athlete with cardiovascular abnormalities: Causes of sudden death, detection by preparticipation screening, and standards for disqualification. *Card. Electrophysiol. Rev. 6*, 100–103.
2. Poetter, K.; et al. (1996) Mutations in either the essential or regulatory light chains of myosin are associated with a rare myopathy in human heart and skeletal muscle. *Nat. Genet. 13* (1), 63–69.
3. Flavigny, J.; et al. (1998) Identification of two novel mutations in the ventricular regulatory myosin light chain gene (MYL2) associated with familial and classical forms of hypertrophic cardiomyopathy. *J. Mol. Med. 76* (3−4), 208–214.
4. Andersen, P. S.; et al. (2001) Myosin light chain mutations in familial hypertrophic cardiomyopathy: Phenotypic presentation and frequency in Danish and South African populations. *J. Med. Genet. 38* (12), E43.
5. Kabaeva, Z. T.; et al. (2002) Systematic analysis of the regulatory and essential myosin light chain genes: Genetic variants and mutations in hypertrophic cardiomyopathy. *Eur. J. Hum. Genet. 10* (11), 741–748.
6. Richard, P.; et al. (2003) Hypertrophic Cardiomyopathy: Distribution of Disease Genes, Spectrum of Mutations, and Implications for a Molecular Diagnosis Strategy. *Circulation 107*, 2227–2232.
7. Morner, S.; et al. (2003) Identification of the genotypes causing hypertrophic cardiomyopathy in northern Sweden. *J. Mol. Cell. Cardiol. 35* (7), 841–849.
8. Hougs, L.; et al. (2005) One third of Danish hypertrophic cardiomyopathy patients have mutations in MYH7 rod region. *Eur. J. Hum. Genet. 13*, 161–165.
9. Kerrick, W. G.; et al. (2009) Malignant familial hypertrophic cardiomyopathy D166V mutation in the ventricular myosin regulatory light chain causes profound effects in skinned and intact papillary muscle fibers from transgenic mice. *FASEB J. 23* (3), 855–865.
10. Abraham, T. P.; et al. (2009) Diastolic dysfunction in familial hypertrophic cardiomyopathy transgenic model mice. *Cardiovasc. Res. 82*, 84–92.
11. Wang, Y.; et al. (2006) Prolonged $Ca^{2+}$ and Force Transients in Myosin RLC Transgenic Mouse Fibers Expressing Malignant and Benign FHC Mutations. *J. Mol. Biol. 361*, 286–299.
12. Oplatka, A. (1972) On the mechanochemistry of muscular contraction. *J. Theor. Biol. 34* (2), 379–403.
13. Dos Remedios, C. G., Millikan, R. G., and Morales, M. F. (1972) Polarization of tryptophan fluorescence from single striated muscle fibers. A molecular probe of contractile state. *J. Gen. Physiol. 59*, 103–120.
14. Dos Remedios, C. G., Yount, R. G., and Morales, M. F. (1972) Individual states in the cycle of muscle contraction. *Proc. Natl. Acad. Sci. U.S.A. 69*, 2542–2546.
15. Nihei, T., Mendelson, R. A., and Botts, J. (1974) Use of fluorescence polarization to observe changes in attitude of S1 moieties in muscle fibers. *Biophys. J. 14*, 236–242.
16. Tregear, R. T., and Mendelson, R. A. (1975) Polarization from a helix of fluorophores and its relation to that obtained from muscle. *Biophys. J. 15*, 455–467.
17. Morales, M. F. (1984) Calculation of the polarized fluorescence from a labeled muscle fiber. *Proc. Natl. Acad. Sci. U.S.A. 81*, 145–149.
18. Sabido-David, C.; et al. (1998) Orientation changes of fluorescent probes at five sites on the myosin regulatory light chain during contraction of single skeletal muscle fibres. *J. Mol. Biol. 279* (2), 387–402.
19. Hopkins, S. C.; et al. (1998) Fluorescence polarization transients from rhodamine isomers on the myosin regulatory light chain in skeletal muscle fibers. *Biophys. J. 74* (6), 3093–3110.
20. Hopkins, S. C.; et al. (2002) Orientation changes of the myosin light chain domain during filament sliding in active and rigor muscle. *J. Mol. Biol. 318* (5), 1275–1291.
21. Elson, E. L., and Magde, D. (1974) Fluorescence Correlation Spectroscopy: Coceptual Basis and Theory. *Biopolymers 13*, 1–28.
22. Elson, E. L. (2004) Quick tour of fluorescence correlation spectroscopy from its inception. *J. Biomed. Opt. 9* (5), 857–864.
23. Bukatina, A. E., Fuchs, F., and Watkins, S. C. (1996) A study on the mechanism of phalloidin-induced tension changes in skinned rabbit psoas muscle fibres. *J. Muscle Res. Cell Motil. 17* (3), 365–371.
24. Prochniewicz-Nakayama, E., Yanagida, T., and Oosawa, F. (1983) Studies on conformation of F-actin in muscle fibers in the relaxed state, rigor, and during contraction using fluorescent phalloidin. *J. Cell Biol. 97*, 1663–1667.
25. Muthu, P.; et al. (2009) Single Molecule Kinetics in the Familial Hypertrophic Cardiomyopathy D166V Mutant Mouse Heart. *J. Mol. Cell. Cardiol. 48* (6), 1264–1271.
26. Mettikolla, P.; et al. (2009) Fluorescence Lifetime of Actin in the FHC Transgenic Heart. *Biochemistry 48* (6), 1264–1271.
27. Herrmann, C.; et al. (1994) Correlation of ActoS1, myofibrillar, and muscle fiber ATPases. *Biochemistry 33* (14), 4148–4154.
28. Borejdo, J.; et al. (2007) Rotation of Actin Monomers during Isometric Contraction of Skeletal Muscle. *J. Biomed. Opt. 12* (1), 014013.
29. Szczesna-Cordary, D.; et al. (2004) Familial hypertrophic cardiomyopathy-linked alterations in $Ca^{2+}$ binding of human cardiac myosin regulatory light chain affect cardiac muscle contraction. *J. Biol. Chem. 279* (5), 3535–3542.
30. Szczesna, D., and Lehrer, S. S. (1993) The binding of fluorescent phallotoxins to actin in myofibrils. *J. Muscle Res. Cell Motil. 14* (6), 594–597.
31. Ao, X., and Lehrer, S. S. (1995) Phalloidin unzips nebulin from thin filaments in skeletal myofibrils. *J. Cell Sci. 108* (Part 11), 3397–3403.
32. Borovikov, Y. S., and Chernogriadskaia, N. A. (1979) Studies on conformational changes in F-actin of glycerinated muscle fibers during relaxation by means of polarized ultraviolet fluorescence microscopy. *Microsc. Acta 81* (5), 383–392.
33. Magde, D., Elson, E. L., and Webb, W. W. (1974) Fluorescence correlation spectroscopy. II. An experimental realization. *Biopolymers 13* (1), 29–61.
34. Elson, E. L. (2008) Introduction to FCS. *Course Cell. Mol. Fluoresc. 2*, 8.
35. Huxley, A. F., and Simmons, R. M. (1971) Proposed mechanism of force generation in striated muscle. *Nature 233*, 533–538.
36. Geeves, M. A., and Holmes, K. C. (2005) The molecular mechanism of muscle contraction. *Adv. Protein Chem. 71* (24), 161–193.
37. Mettikolla, P. (2010) Kinetics of a Single Cross-Bridge in a Familial Hypertrophic Cardiomyopathy Heart Muscle Measured by Reverse Kretschmann Fluorescence. *J. Biomed. Opt. 15*, No. 017011.
38. Maass, A., and Leinwand, L. A. (2000) Animal models of hypertrophic cardiomyopathy. *Curr. Opin. Cardiol. 15*, 189–196.
39. Greenberg, M. J.; et al. (2009) Regulatory light chain mutations associated with cardiomyopathy affect myosin mechanics and kinetics. *J. Mol. Cell. Cardiol. 46* (1), 108–115.